Automatic scaling of critical frequency foF2 *from ionograms recorded at São José dos Campos, Brazil: a comparison between Autoscala and UDIDA tools*

Michael Pezzopane, Valdir Gil Pillat & Paulo Roberto Fagundes

Acta Geophysica

ISSN 1895-6572

Acta Geophys.
DOI 10.1007/s11600-017-0015-z

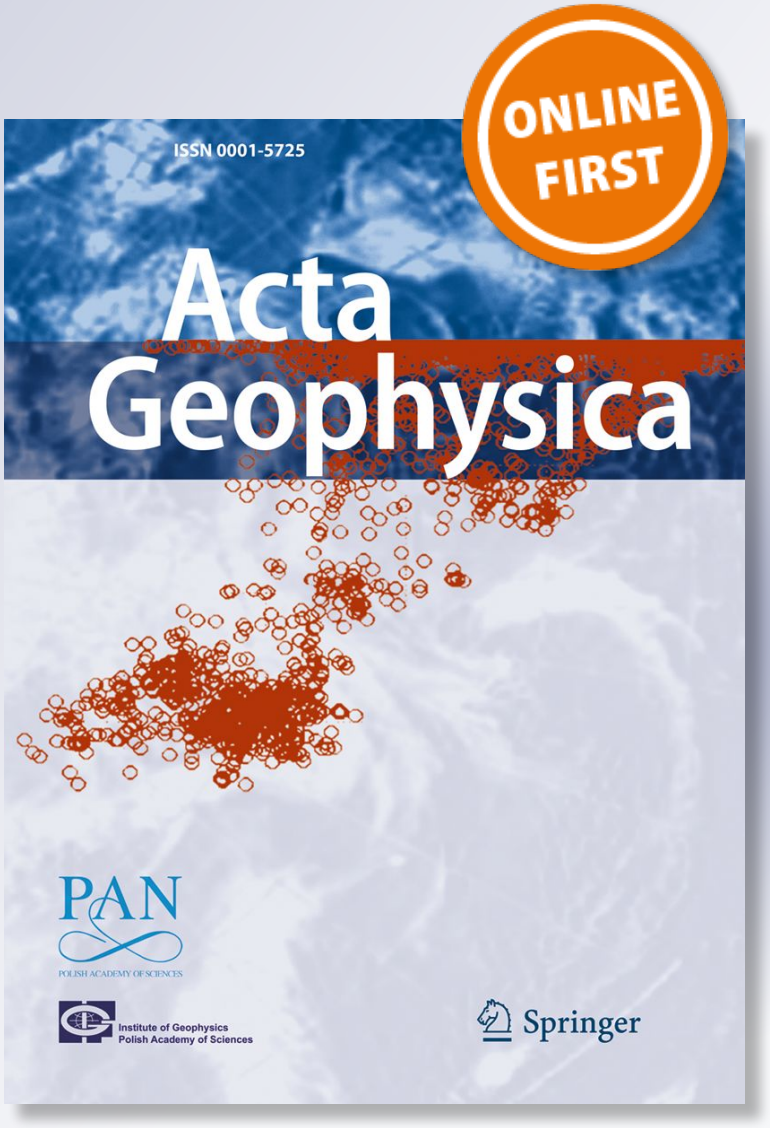

Springer

Acta Geophys.
DOI 10.1007/s11600-017-0015-z

RESEARCH ARTICLE

Automatic scaling of critical frequency *fo*F2 from ionograms recorded at São José dos Campos, Brazil: a comparison between Autoscala and UDIDA tools

Michael Pezzopane[1] · Valdir Gil Pillat[2] · Paulo Roberto Fagundes[2]

Received: 23 January 2017 / Accepted: 27 January 2017

Abstract This paper considers a dataset of ionograms recorded by the CADI ionosonde installed at São José dos Campos (SJC; 23.2°S, 45.9°W, magnetic latitude 14.1°S), Brazil, to compare two autoscaling systems: Autoscala, developed by the Istituto Nazionale di Geofisica e Vulcanologia, and the UDIDA-scaling, developed by the Universidade do Vale do Paraíba. The analysis, focused on the critical frequency of the F2 layer, *fo*F2, shows that the two systems work differently. The UDIDA-scaling gives always a value of *fo*F2 as output, regardless of the presence of the ionogram trace and its definition, while Autoscala tends to reject ionograms for which the digital information is considered insufficient. As a consequence, the UDIDA-scaling can autoscale more *fo*F2 values than Autoscala, but Autoscala can discard a larger number of ionograms for which the trace is unidentifiable. Discussions are made on the accuracy of the *fo*F2 values given as output, as well as on the main shortcomings characterizing the two systems.

Keywords Ionogram · Ionosonde · Low-latitude ionosphere · Critical frequency *fo*F2 · Automatic scaling

✉ Michael Pezzopane
michael.pezzopane@ingv.it

Valdir Gil Pillat
valdirgp@univap.br

Paulo Roberto Fagundes
fagundes@univap.br

[1] Istituto Nazionale di Geofisica e Vulcanologia, Rome, Italy

[2] Laboratório de Física e Astronomia, Universidade do Vale do Paraíba (UNIVAP), São José dos Campos, São Paulo, Brazil

Introduction

The importance of recording real-time vertical sounding data, especially for space weather purposes, has greatly increased over the past years. In particular, the assimilation of this kind of data into ionospheric models has become more and more important (Pezzopane et al. 2011, 2013; Galkin 2012; Lee et al. 2012; McNamara et al. 2013; Gardner et al. 2014; Chartier et al. 2016; Sabbagh et al. 2016). For this reason, in the last decades, several groups of researchers worked hard to implement systems able to automatically scale the experimental trace obtained after performing an ionospheric vertical sounding, that is, an ionogram (Reinisch and Huang 1983; Fox and Blundell 1989; Igi et al. 1993; Tsai and Berkey 2000; Zabotin et al. 2006; Ding et al. 2007; Galkin and Reinisch 2008; Su et al. 2012; Chen et al. 2013; Zheng et al. 2013; Jiang et al. 2013, 2014, 2015a, b). In particular, the ARTIST system developed by the University of Lowell, Center for Atmospheric Research, has been widely used and tested (Gilbert and Smith 1988; Conkright and McNamara 1997; Jacobs et al. 2004; Reinisch et al. 2005; McNamara 2006; Bamford et al. 2008; Stankov et al. 2012). Although much progress has been made, there are many issues that have still to be faced, and a significant work is being continuously made to upgrade existing programs. The aim of these improvements is, on the one hand, to advance the reliability of the automatically scaled data, and on the other hand to adapt some systems for being installed in ionosondes that are not equipped with a tool to automatically scale the recorded trace.

One type of ionosonde that is built without being equipped with an automatic scaling system is the Canadian Advanced Digital Ionosonde (CADI) (MacDougall 1993). The present paper considers a dataset of ionograms

Published online: 08 February 2017

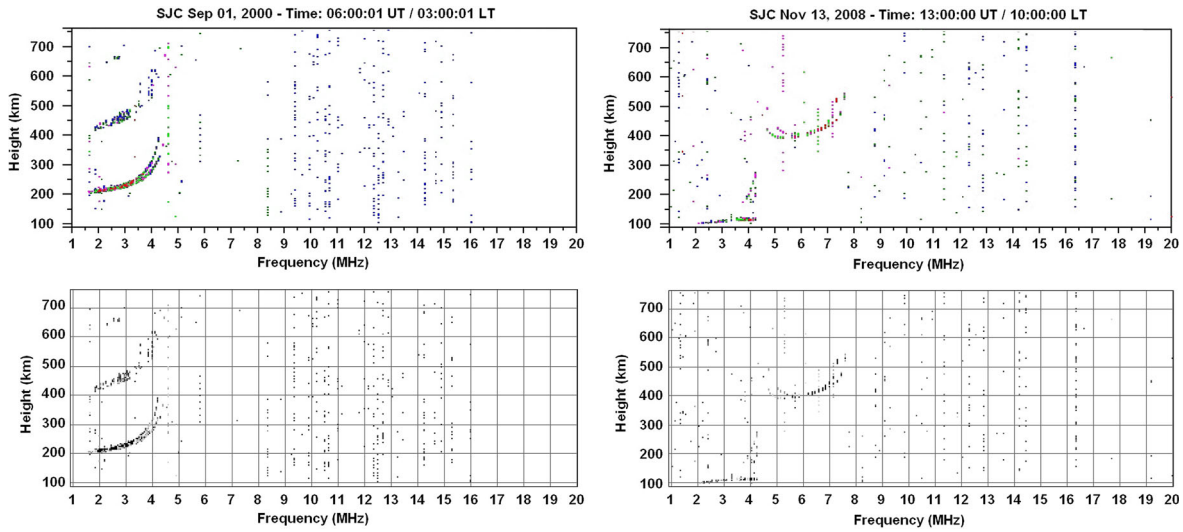

Fig. 1 Examples of conversion from (*top*) the MD4 format to (*bottom*) the RDF format for ionograms recorded at SJC on (*left*) 1 September 2000 at 06:00 UT and (*right*) 13 November 2008 at 13:00 UT

Table 1 The autoscaling statistics (see the text for the description of the four different subsets), and the corresponding autoscaling accuracy for subset 1, are shown for both Autoscala and UDIDA for the hourly ionograms recorded in September 2000 ($R_{12} = 116$)

September 2000 ($R_{12} = 116$) (603 ionograms)		
Autoscaling statistics		
	Autoscala	UDIDA
Subset 1	137 (~37%)	369
Subset 2	229 (~98%)	–
Subset 3	5 (~2%)	234
Subset 4	232 (~63%)	–

Autoscaling accuracy subset 1						
x_a = |autoscaled value − validated value| (MHz)	Autoscala (137 ionograms)			UDIDA (369 ionograms)		
	Total ionograms (137)	Daytime ionograms (59)	Nighttime ionograms (78)	Total ionograms (369)	Daytime ionograms (242)	Nighttime ionograms (127)
$x_a \leq 0.5$	127 (~93%)	53 (~90%)	74 (~95%)	265 (~72%)	165 (~68%)	100 (~79%)
$0.5 < x_a \leq 1.0$	5 (~3%)	2 (~3%)	3 (~4%)	52 (~14%)	37 (~15%)	15 (~12%)
$1.0 < x_a \leq 1.5$	–	–	–	35 (~10%)	28 (~12%)	7 (~5%)
$x_a > 1.5$	5 (~3%)	4 (~7%)	1 (~3%)	17 (~4%)	12 (~5%)	5 (~4%)
x_r = |autoscaled value − validated value|/validated value	Autoscala (137 ionograms)			UDIDA (369 ionograms)		
	Total ionograms (137)	Daytime ionograms (59)	Nighttime ionograms (78)	Total ionograms (369)	Daytime ionograms (242)	Nighttime ionograms (127)
$x_r \leq 0.1$	130 (~95%)	55 (~93%)	75 (~96%)	328 (~89%)	221 (~91%)	107 (~84%)
$0.1 < x_r \leq 0.3$	3 (~2%)	1 (~2%)	2 (~3%)	35 (~9%)	17 (~7%)	18 (~14%)
$0.3 < x_r \leq 0.5$	3 (~2%)	2 (~3%)	1 (~1%)	3 (~1%)	1 (~1%)	2 (~2%)
$x_r > 0.5$	1 (~1%)	1 (~2%)	–	3 (~1%)	3 (~1%)	–

Concerning the "Autoscaling statistics": the percentages between brackets of Autoscala for subset 1 and subset 4 refer to the total number of ionograms of (subset 1 + subset 4), that is, the ionograms for which the operator gave a value of *fo*F2 as output; the percentages between brackets of Autoscala for subset 2 and subset 3 refer to the total number of ionograms of (subset 2 + subset 3), that is, the ionograms for which the operator did not give any value of *fo*F2 as output

Table 2 Same as Table 1 but for March 2004 ($R_{12} = 47$)

March 2004 ($R_{12} = 47$) (627 ionograms)						
Autoscaling statistics						
	Autoscala			UDIDA		
Subset 1	265 (~51%)			522		
Subset 2	85 (~81%)			–		
Subset 3	20 (~19%)			105		
Subset 4	257 (~49%)			–		
Autoscaling accuracy subset 1						
x_a = |autoscaled value − validated value| (MHz)	Autoscala (265 ionograms)			UDIDA (522 ionograms)		
	Total ionograms (265)	Daytime ionograms (125)	Nighttime ionograms (140)	Total ionograms (522)	Daytime ionograms (316)	Nighttime ionograms (206)
$x_a \leq 0.5$	241 (~91%)	110 (~88%)	131 (~94%)	278 (~53%)	183 (~58%)	95 (~46%)
$0.5 < x_a \leq 1.0$	20 (~7%)	11 (~8%)	9 (~6%)	109 (~21%)	62 (~20%)	47 (~22%)
$1.0 < x_a \leq 1.5$	2 (~1%)	2 (~2%)	–	87 (~17)	55 (~17%)	32 (~16%)
$x_a > 1.5$	2 (~1%)	2 (~2%)	–	48 (~8%)	16 (~5%)	32 (~16%)
x_r = |autoscaled value − validated value|/validated value	Autoscala (265 ionograms)			UDIDA (522 ionograms)		
	Total ionograms (265)	Daytime ionograms (125)	Nighttime ionograms (140)	Total ionograms (522)	Daytime ionograms (316)	Nighttime ionograms (206)
$x_r \leq 0.1$	247 (~93%)	117 (~94%)	130 (~93%)	379 (~73%)	261 (~83%)	118 (~57%)
$0.1 < x_r \leq 0.3$	18 (~7%)	8 (~6%)	10 (~7%)	94 (~18%)	43 (~13%)	51 (~25%)
$0.3 < x_r \leq 0.5$	–	–	–	30 (~6%)	8 (~3%)	22 (~11%)
$x_r > 0.5$	–	–	–	19 (~3%)	4 (~1%)	15 (~7%)

recorded by the CADI ionosonde installed at São José dos Campos (SJC) (23.2°S, 45.9°W, magnetic latitude 14.1°S), Brazil, and discusses the results obtained after applying two different autoscaling systems, Autoscala, developed at Istituto Nazionale di Geofisica e Vulcanologia, Rome, Italy (Pezzopane and Scotto 2005, 2007, 2010), and the UNIVAP Digital Ionosonde Data Analysis-scaling (UDIDA-scaling, hereafter UDIDA), developed at the Laboratório de Física e Astronomia of the Universidade do Vale do Paraíba (UNIVAP), São José dos Campos, Brazil (Pillat et al. 2013).

The main characteristic of Autoscala is that it is based on an image recognition technique, which makes the algorithm unrelated to the hardware features of the ionosonde, and consequently able to scale ionograms independently of the information on the polarization tagging. The algorithm gives as output the main characteristics of the F2, F1, E, and Es ionospheric layers, as well as an estimation of the vertical electron density profile (Scotto 2009), and it has been applied to different types of ionosonde (Pezzopane and Scotto 2004; Scotto and Pezzopane 2008; Bullett et al. 2010; Krasheninnikov et al. 2010; Pezzopane et al. 2010; Scotto and MacDougall 2012; Enell et al. 2016).

UDIDA uses a fuzzy relation to fit the trace and gives as output the following F region characteristics: the critical frequency of the F region (*fo*F2), the virtual height of the base of the F region (h'F), and the F region peak height (*hp*F2 = h(*fo*F2·0.834)) (Piggott and Rawer 1972).

In this paper, ionograms recorded at SJC for quiet and disturbed periods are autoscaled by both Autoscala and UDIDA. The dataset considered, how the data analysis has been carried out, and the corresponding results are described in the next section followed by which discussion is given. Conclusions are given in the final section.

Datasets, analyses and results

The ionograms considered to compare the two autoscaling systems, Autoscala and UDIDA, are divided into two groups. The first group includes the hourly ionograms recorded at SJC

Table 3 Same as Table 1 but for November 2008 ($R_{12} = 2$)

November 2008 ($R_{12} = 2$) (510 ionograms)						
Autoscaling statistics						
	Autoscala			UDIDA		
Subset 1	228 (~53%)			428		
Subset 2	61 (~74%)			–		
Subset 3	21 (~26%)			82		
Subset 4	200 (~47%)			–		
Autoscaling accuracy subset 1						
x_a = |autoscaled value − validated value| (MHz)	Autoscala (228 ionograms)			UDIDA (428 ionograms)		
	Total ionograms (228)	Daytime ionograms (93)	Nighttime ionograms (135)	Total ionograms (428)	Daytime ionograms (234)	Nighttime ionograms (194)
$x_a \leq 0.5$	224 (~98%)	93 (100%)	131 (~97%)	270 (~63%)	153(~65%)	117 (~60%)
$0.5 < x_a \leq 1.0$	4 (~2%)	–	4 (~3%)	47 (~11%)	18 (~8%)	29 (~15%)
$1.0 < x_a \leq 1.5$	–	–	–	31 (~7%)	14 (~6%)	17 (~9%)
$x_a > 1.5$	–	–	–	80 (~19%)	49 (~21%)	31 (~16%)
x_r = |autoscaled value − validated value|/validated value	Autoscala (228 ionograms)			UDIDA (428 ionograms)		
	Total ionograms (228)	Daytime ionograms (93)	Nighttime ionograms (135)	Total ionograms (428)	Daytime ionograms (234)	Nighttime ionograms (194)
$x_r \leq 0.1$	219 (~96%)	92 (~99%)	127 (~94%)	282 (~66%)	168 (~72%)	114 (~59%)
$0.1 < x_r \leq 0.3$	9 (~4%)	1 (~1%)	8 (~6%)	73 (~17%)	28 (~12%)	45 (~23%)
$0.3 < x_r \leq 0.5$	–	–	–	26 (~6%)	14 (~6%)	12 (~6%)
$x_r > 0.5$	–	–	–	47 (~11%)	24 (~10%)	23 (~12%)

for high solar activity ($R_{12} = 116$) in September 2000, for medium solar activity ($R_{12} = 47$) in March 2004, and for low solar activity ($R_{12} = 2$) in November 2008, and it represents the "quiet" dataset, even though a geomagnetic storm occurred during 17–20 September 2000 ($D_{st} = -201$ nT). The second group, which represents the "disturbed" dataset, includes the 5-min ionograms recorded at SJC during three different geomagnetic storms that occurred during 24–26 August 2005 ($D_{st} = -184$ nT), during 14–16 December 2006 ($D_{st} = -162$ nT), and during 24–26 October 2011 ($D_{st} = -147$ nT), and during the well-known and well-studied St. Patrick storm that occurred during 17–19 March 2015 ($D_{st} = -223$ nT) (Astafyeva et al. 2015; Carter et al. 2016; De Michelis et al. 2016; Nava et al. 2016; Nayak et al. 2016; Pignalberi et al. 2016; Spogli et al. 2016; Tulasi Ram et al. 2016; Zhong et al. 2016).

It is worth highlighting that to process CADI ionograms with Autoscala it was necessary to perform an ionogram file format conversion from the MD4 one, which is the native CADI format, to the RDF format (Pezzopane 2004), which is the format with which the Autoscala system was run since the early stage of its development. This format conversion did not cause any loss of information, as it is shown in Fig. 1 for typical nighttime and daytime ionograms.

To evaluate the two autoscaling systems, automatically scaled values of *fo*F2 are compared with the ones hand-scaled by an experienced operator. We chose to carry out the test by considering the ionospheric characteristic *fo*F2 because for this one both systems obtained the most reliable results. Moreover, with reference to the processing dataset of ionograms, the following subsets were considered: subset 1, including ionograms for which both the autoscaling system and the operator give a value as output; subset 2, including ionograms for which neither the autoscaling system nor the operator give a value as output; subset 3, including ionograms for which the autoscaling system gives a value as output, while the operator does not; subset 4, including ionograms for which the operator gives a value as output, while the autoscaling system does not.

Tables 1, 2, 3, 4, 5, 6 and 7 show the results obtained after applying both Autoscala and UDIDA on each of the seven single periods (the three quiet months and the four disturbed periods) forming the whole considered dataset of ionograms recorded at SJC. For each table, the top part

Table 4 Same as Table 1 but for the 5-min ionograms recorded during 24–26 August 2005, a disturbed period characterized by a D_{st} of −184 nT

Storm 24–26 August 2005 (D_{st} = −184 nT) (826 ionograms)		
Autoscaling statistics		
	Autoscala	UDIDA
Subset 1	507 (∼80%)	635
Subset 2	122 (∼64%)	–
Subset 3	69 (∼36%)	191
Subset 4	128 (∼20%)	–

Autoscaling accuracy subset 1						
x_a = |autoscaled value − validated value| (MHz)	Autoscala (507 ionograms)			UDIDA (635 ionograms)		
	Total ionograms (507)	Daytime ionograms (254)	Nighttime ionograms (253)	Total ionograms (635)	Daytime ionograms (362)	Nighttime ionograms (273)
$x_a \leq 0.5$	493 (∼97%)	248 (∼97%)	245 (∼97%)	325 (∼51%)	212 (∼59%)	113 (∼41%)
$0.5 < x_a \leq 1.0$	11 (∼2%)	4 (∼2%)	7 (∼2%)	124 (∼20%)	62 (∼17%)	62 (∼23%)
$1.0 < x_a \leq 1.5$	1 (∼0.5%)	–	1 (∼1%)	78 (∼12%)	19 (∼5%)	59 (∼22%)
$x_a > 1.5$	2 (∼0.5%)	2 (∼1%)	–	108 (∼17%)	69 (∼19%)	39 (∼14%)
x_r = |autoscaled value – validated value|/validated value	Autoscala (507 ionograms)			UDIDA (635 ionograms)		
	Total ionograms (507)	Daytime ionograms (254)	Nighttime ionograms (253)	Total ionograms (635)	Daytime ionograms (362)	Nighttime ionograms (273)
$x_r \leq 0.1$	488 (∼96%)	249 (∼98%)	239 (∼94%)	338 (∼53%)	239 (∼66%)	99 (∼36%)
$0.1 < x_r \leq 0.3$	19 (∼4%)	5 (∼2%)	14 (∼6%)	150 (∼24%)	63 (∼17%)	87 (∼32%)
$0.3 < x_r \leq 0.5$	–	–	–	72 (∼11%)	24 (∼7%)	48 (∼18%)
$x_r > 0.5$	–	–	–	75 (∼12%)	36 (∼10%)	39 (∼14%)

(named as "Autoscaling statistics") shows the number of ionograms falling in each subset (1, 2, 3 or 4), while the bottom part (named as "Autoscaling accuracy subset 1") shows the autoscaling accuracy related to subset 1, in terms of four different ranges ($x_a \leq 0.5$, $0.5 < x_a \leq 1.0$, $1.0 < x_a \leq 1.5$, and $x_a > 1.5$) of the absolute error x_a = |autoscaled value − validated value|, and in terms of 4 different ranges ($x_r \leq 0.1$, $0.1 < x_r \leq 0.3$, $0.3 < x_r \leq 0.5$, and $x_r > 0.5$) of the relative error x_r = (|autoscaled value − validated value|/validated value). In both cases, a distinction between daytime ionograms (recorded between 6:00 and 18:00 LT) and nighttime ionograms (recorded between 18:00 and 6:00 LT) was also made.

Moreover, for each of the seven considered periods, corresponding linear fits between autoscaled and validated values of subset 1 are shown for Autoscala and UDIDA in Figs. 2 and 3, for quiet and disturbed periods, respectively; the number visible at the bottom right corner of each plot is the Pearson correlation coefficient, according to the following formula

$$\rho_{X,Y} = \frac{\mathrm{cov}(X,Y)}{\sigma_X \sigma_Y} = \frac{E((X - E(X))(Y - E(Y)))}{\sigma_X \sigma_Y}, \quad (1)$$

where cov() is the covariance between the variables X and Y, σ_X and σ_Y are the corresponding standard deviations, and $E()$ represents the expected value. Specifically, to compare the performances of both autoscaling systems at the same level, besides showing the linear fits for the whole subset 1 of Autoscala (left columns of plots) and for the whole subset 1 of UDIDA (right column of plots), Figs. 2 and 3 show also the linear fits for the part of subset 1 of UDIDA, which is coincident with the subset 1 of Autoscala (middle column of plots).

Discussion

Looking at Tables 1, 2, 3, 4, 5, 6 and 7, the different philosophy characterizing the two autoscaling systems is evident. On the one hand, UDIDA gives always a value for

Table 5 Same as Table 1 but for the 5-min ionograms recorded during 14–16 December 2006, a disturbed period characterized by a D_{st} of −162 nT

Storm 14–16 December 2006 (D_{st} = −162 nT) (860 ionograms)						
Autoscaling statistics						
	Autoscala			UDIDA		
Subset 1	316 (∼48%)			658		
Subset 2	133 (∼66%)			–		
Subset 3	69 (∼34%)			202		
Subset 4	342 (∼52%)			–		
Autoscaling accuracy subset 1						
x_a = |autoscaled value − validated value| (MHz)	Autoscala (316 ionograms)			UDIDA (658 ionograms)		
	Total ionograms (316)	Daytime ionograms (157)	Nighttime ionograms (159)	Total ionograms (658)	Daytime ionograms 423)	Nighttime ionograms (235)
$x_a \leq 0.5$	292 (∼92%)	140 (∼89%)	152 (∼96%)	300 (∼46%)	195 (∼46%)	105 (∼45%)
$0.5 < x_a \leq 1.0$	22 (∼7%)	15 (∼9%)	7 (∼4%)	101 (∼15%)	62 (∼15%)	39 (∼17%)
$1.0 < x_a \leq 1.5$	1 (∼0.5%)	1 (∼1%)	–	73 (∼11%)	46 (∼11%)	27 (∼11%)
$x_a > 1.5$	1 (∼0.5%)	1 (∼1%)	–	184 (∼28%)	120 (∼28%)	64 (∼27%)
x_r = |autoscaled value − validated value|/validated value	Autoscala (316 ionograms)			UDIDA (658 ionograms)		
	Total ionograms (316)	Daytime ionograms (157)	Nighttime ionograms (159)	Total ionograms (658)	Daytime ionograms (423)	Nighttime ionograms (235)
$x_r \leq 0.1$	296 (∼93%)	144 (∼92%)	152 (∼96%)	367 (∼56%)	256 (∼61%)	111 (∼47%)
$0.1 < x_r \leq 0.3$	19 (∼6%)	12 (∼7%)	7 (∼4%)	168 (∼25%)	106 (∼25%)	62 (∼27%)
$0.3 < x_r \leq 0.5$	1 (∼1%)	1 (∼1%)	–	56 (∼9%)	27 (∼6%)	29 (∼12%)
$x_r > 0.5$	–	–	–	67 (∼10%)	34 (∼8%)	33 (∼14%)

*fo*F2, independently of the presence of the ionogram trace and, if present, independently of its definition; on the other hand, Autoscala tends to discard ionograms for which the digital information is considered insufficient, giving no value of *fo*F2 as output. This different kind of processing explains why the number of ionograms falling in the subset 1 is greater for UDIDA than for Autoscala, while the number of ionograms falling in the subset 4 is greater for Autoscala than for UDIDA. In fact, for both quiet and disturbed conditions, and independent of the solar activity, the trace referring to the F2 layer is weak and scarcely defined for most of the ionograms, and consequently Autoscala does not give any *fo*F2 value as output. As an example, Fig. 4 shows an ionogram for which the operator scaled a value of 11.0 MHz for *fo*F2, while Autoscala considered the digital information insufficient to identify the ionogram trace. This Autoscala behavior might be smoothed by varying the thresholds used by the algorithm to identify the F2 trace, but this is a long and hard task that could be done as a further step.

At the same time, however, this feature allows Autoscala to identify correctly the ionogram cases for which the operator did not validate any *fo*F2 value, and in fact the number of ionograms falling in the subset 2 for Autoscala is high. On the contrary, UDIDA cannot identify this kind of ionograms, and correspondingly the number of ionograms falling in the subset 3 is large. This is a feature of UDIDA that has to be certainly improved in the near future, namely this system should be equipped with a subroutine able to reliably identify whether the ionogram trace is absent or not.

Figures 5 and 6 show two examples of ionograms falling in the subsets 1 and 3, respectively, as processed by Autoscala and UDIDA.

Concerning the number of ionograms falling in subset 3, this shows a tendency to increase for both Autoscala and

Table 6 Same as Table 1 but for the 5-min ionograms recorded during 24–26 October 2011, a disturbed period characterized by a D_{st} of −147 nT

Storm 24–26 October 2011 (D_{st} = −147 nT) (761 ionograms)		
Autoscaling statistics		
	Autoscala	UDIDA
Subset 1	103 (∼19%)	539
Subset 2	203 (∼91%)	–
Subset 3	19 (∼9%)	222
Subset 4	436 (∼81%)	–

Autoscaling accuracy subset 1						
x_a = |autoscaled value − validated value| (MHz)	Autoscala (103 ionograms)			UDIDA (539 ionograms)		
	Total ionograms (103)	Daytime ionograms (55)	Nighttime ionograms (48)	Total ionograms (539)	Daytime ionograms (391)	Nighttime ionograms (148)
$x_a \leq 0.5$	84 (∼82%)	37 (∼67%)	47 (∼98%)	253 (∼47%)	192 (∼49%)	61 (∼41%)
$0.5 < x_a \leq 1.0$	10 (∼10%)	9 (∼16%)	1 (∼2%)	137 (∼25%)	92 (∼24%)	45 (∼30%)
$1.0 < x_a \leq 1.5$	2 (∼1%)	2 (∼4)	–	100 (∼19%)	71 (∼18%)	29 (∼20%)
$x_a > 1.5$	7 (∼7%)	7 (∼13%)	–	49 (∼9%)	36 (∼9%)	13 (∼9%)
x_r = |autoscaled value − validated value|/validated value	Autoscala (103 ionograms)			UDIDA (539 ionograms)		
	Total ionograms (103)	Daytime ionograms (55)	Nighttime ionograms (48)	Total ionograms (539)	Daytime ionograms (391)	Nighttime ionograms (148)
$x_r \leq 0.1$	92 (∼89%)	44 (∼80%)	48 (100%)	424 (∼79%)	314 (∼80%)	110 (∼74%)
$0.1 < x_r \leq 0.3$	9 (∼9%)	9 (∼16%)	–	102 (∼18%)	70 (∼18%)	32 (∼22%)
$0.3 < x_r \leq 0.5$	1 (∼1%)	1 (∼2%)	–	9 (∼2%)	4 (∼1%)	5 (∼3%)
$x_r > 0.5$	1 (∼1%)	1 (∼2%)	–	4 (∼1%)	3 (∼1%)	1 (∼1%)

UDIDA for disturbed periods. For Autoscala, also the number of ionograms falling in the subset 4 seems to increase for disturbed periods.

Concerning the number of ionograms falling in the subset 1, for both UDIDA and Autoscala it seems to be independent of both the period and the solar activity.

Focusing the attention on the accuracy of the autoscaling of ionograms of subset 1, this is very high for Autoscala, regardless of both the considered period and the solar activity, while for UDIDA it decreases for disturbed periods. Moreover, Tables 1, 2, 3, 4, 5, 6 and 7 show also that the accuracy of the UDIDA autoscaling seems to slightly decrease for nighttime ionograms. As it is shown in Fig. 7, this is mainly due to the occurrence of multiple reflections of the sporadic E (Es) layer and the presence of noise, which mislead the algorithm, causing as a consequence large absolute and relative errors.

The high accuracy characterizing the autoscaling made by Autoscala can be also inferred by looking at Figs. 2 and 3, where the linear fits related to Autoscala are all very good, with values of the Pearson correlation coefficient ranging from 0.87 to 0.99. This means that when Autoscala gives a value of *fo*F2 as output, this is very reliable.

Instead, the linear fits related to UDIDA, except the cases of September 2000 and March 2004, are worse than those related to Autoscala, showing a more significant spread of the points, with values of the Pearson correlation coefficient that are lower, especially for disturbed periods.

The main causes of error for UDIDA are then: (1) the presence of spread-F (Fig. 6); (2) the presence of noise (Fig. 7a); (3) the appearance of multiple reflections of the sporadic E layer (Fig. 7b); (4) the appearance of multiple reflections of the F layer (Fig. 8). Concerning (1), UDIDA

Table 7 Same as Table 1 but for the 5-min ionograms recorded during 17–19 March 2015, a disturbed period characterized by a D_{st} of −223 nT

St. Patrick storm 17–19 March 2015 (D_{st} = −223 nT) (864 ionograms)		
Autoscaling statistics		
	Autoscala	UDIDA
Subset 1	269 (∼46%)	613
Subset 2	216 (∼86%)	–
Subset 3	35 (∼14%)	251
Subset 4	344 (∼57%)	–

Autoscaling accuracy subset 1						
x = lautoscaled value − validated valuel (MHz)	Autoscala (269 ionograms)			UDIDA (613 ionograms)		
	Total ionograms (269)	Daytime ionograms (135)	Nighttime ionograms (134)	Total ionograms (613)	Daytime ionograms (352)	Nighttime ionograms (261)
$x \leq 0.5$	250 (∼93%)	125 (∼93%)	125 (∼93%)	238 (∼39%)	143 (∼41%)	95 (∼36%)
$0.5 < x \leq 1.0$	16 (∼6%)	7 (∼5%)	9 (∼7%)	110 (∼18%)	59 (∼17%)	51 (∼20%)
$1.0 < x \leq 1.5$	3 (∼1%)	3 (∼2%)	–	97 (∼16%)	68 (∼19%)	29 (∼11%)
$x > 1.5$	–	–	–	168 (∼27%)	82 (∼23%)	86 (∼33%)

x = lautoscaled value − validated valuel/validated value	Autoscala (269 ionograms)			UDIDA (613 ionograms)		
	Total ionograms (269)	Daytime ionograms (135)	Nighttime ionograms (134)	Total ionograms (613)	Daytime ionograms (352)	Nighttime ionograms (261)
$x \leq 0.1$	252 (∼94%)	129 (∼96%)	123 (∼92%)	357 (∼58%)	229 (∼65%)	128 (∼49%)
$0.1 < x \leq 0.3$	17 (∼6%)	6 (∼4%)	11 (∼8%)	146 (∼24%)	84 (∼24%)	62 (∼24%)
$0.3 < x \leq 0.5$	–	–	–	50 (∼8%)	24 (∼7%)	26 (∼10%)
$x > 0.5$	–	–	–	60 (∼10%)	15 (∼4%)	45 (∼17%)

considers the trace definite enough even though it is characterized by a strong spread-F phenomenon which induces unreliable *fo*F2 values; concerning (2), the presence of clusters of points due to noise causes a wrong identification of the trace and a consequent overestimation of the value given as output; concerning (3) and (4), UDIDA is misled by traces that are not those of the real ionogram. A significant effort has been invested by the UDIDA research team to smooth such errors (Pillat et al. 2015).

Autoscala instead can manage quite well the presence of multiple reflections (Scotto and Pezzopane 2008), and the main causes of error are: (1) a pronounced weakness of the trace (Fig. 4); (2) the presence of spread-F (Fig. 6); (3) the appearance of additional stratifications of the F layer (Lynn et al. 2000; Fagundes et al. 2007) (Fig. 9). Concerning (1), as it was previously mentioned, this malfunctioning of Autoscala might be mitigated by working on thresholds used by the algorithm; concerning (2), it is worth highlighting that most of the ionograms characterized by spread-F phenomena are correctly identified by Autoscala as not identifiable; concerning (3), the problem is known (Scotto 2009) and more complex to be fixed, because it implies a reconsideration of the empirical curves used by Autoscala to identify the different parts of the ionogram; at the same time, Fig. 9 shows that UDIDA can manage better than Autoscala the presence of additional stratifications of the F layer.

Conclusions

By considering ionograms recorded by the CADI ionosonde installed at SJC, for quiet and disturbed periods, two autoscaling systems, Autoscala and UDIDA, were compared. UDIDA gives a value of *fo*F2 for each analyzed ionogram, while Autoscala tends to reject ionograms for which the digital information is considered

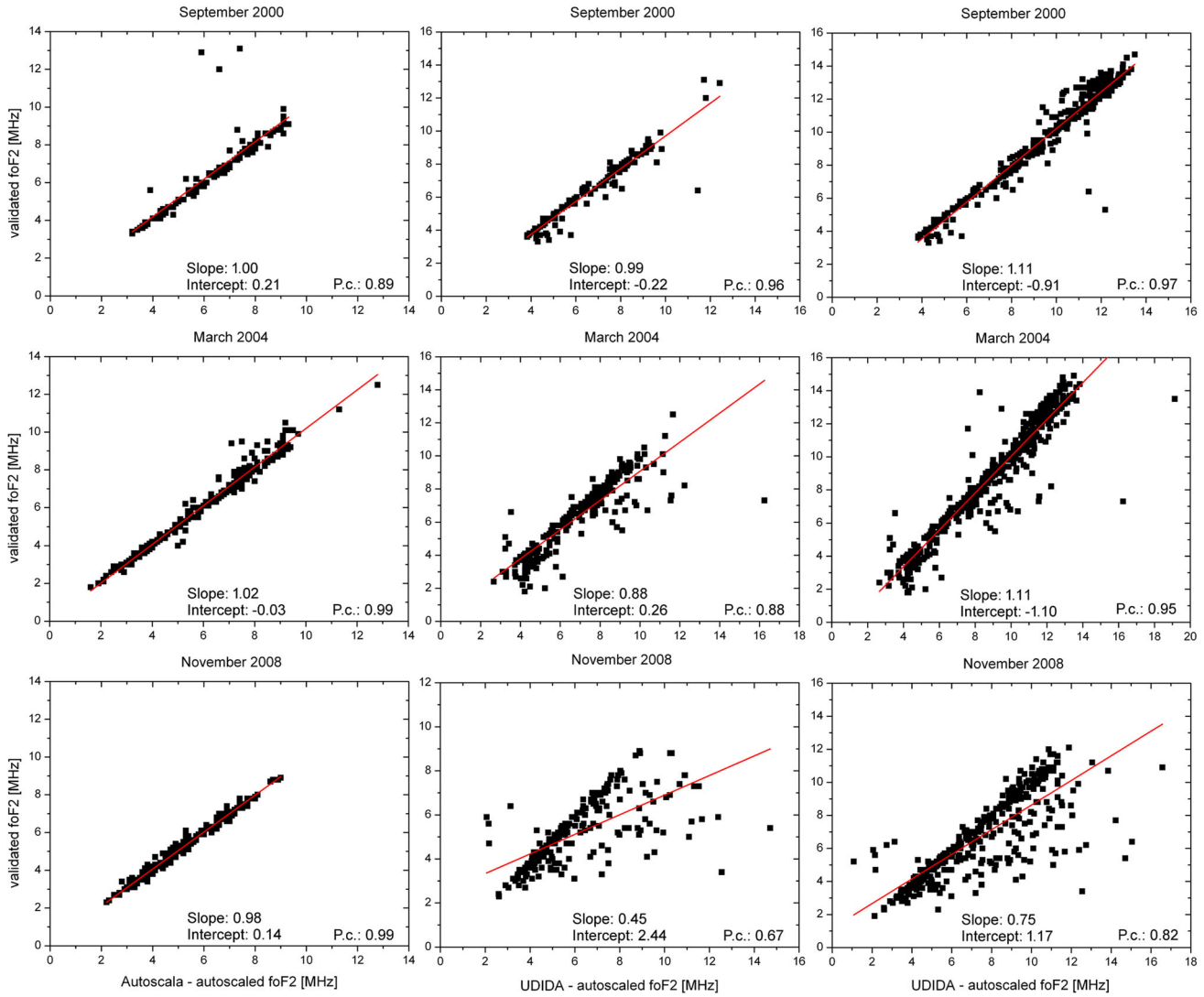

Fig. 2 Linear fits (in *red* the regression line, the slope and the intercept values of which are reported at the *bottom* of each plot) for the whole subset 1 (see the text for the description of the four different subsets) of Autoscala (*left column*), for the whole subset 1 of UDIDA (*right column*), and for the part of subset 1 of UDIDA, which is coincident with the subset 1 of Autoscala (*middle column*), for the quiet periods of September 2000, March 2004, and November 2008. The value of the Pearson correlation coefficient is reported at the *bottom right corner* of each plot

insufficient, and no value of *fo*F2 is given as output. This means that UDIDA can give more *fo*F2 values as output than Autoscala, and that Autoscala can correctly discard a large number of ionograms for which the operator does not validate any *fo*F2 value. With regard to the dependence of the autoscaling on the period and the solar activity, when the operator validates a value of *fo*F2, the capacity of both autoscaling systems in giving a value as output does not present any kind of pattern. Instead, the rejection made by Autoscala for ionograms validated by an operator seems to increase for disturbed conditions. The same pattern seems to characterize the number of ionograms not validated by an operator and incorrectly autoscaled by both systems. The accuracy of the

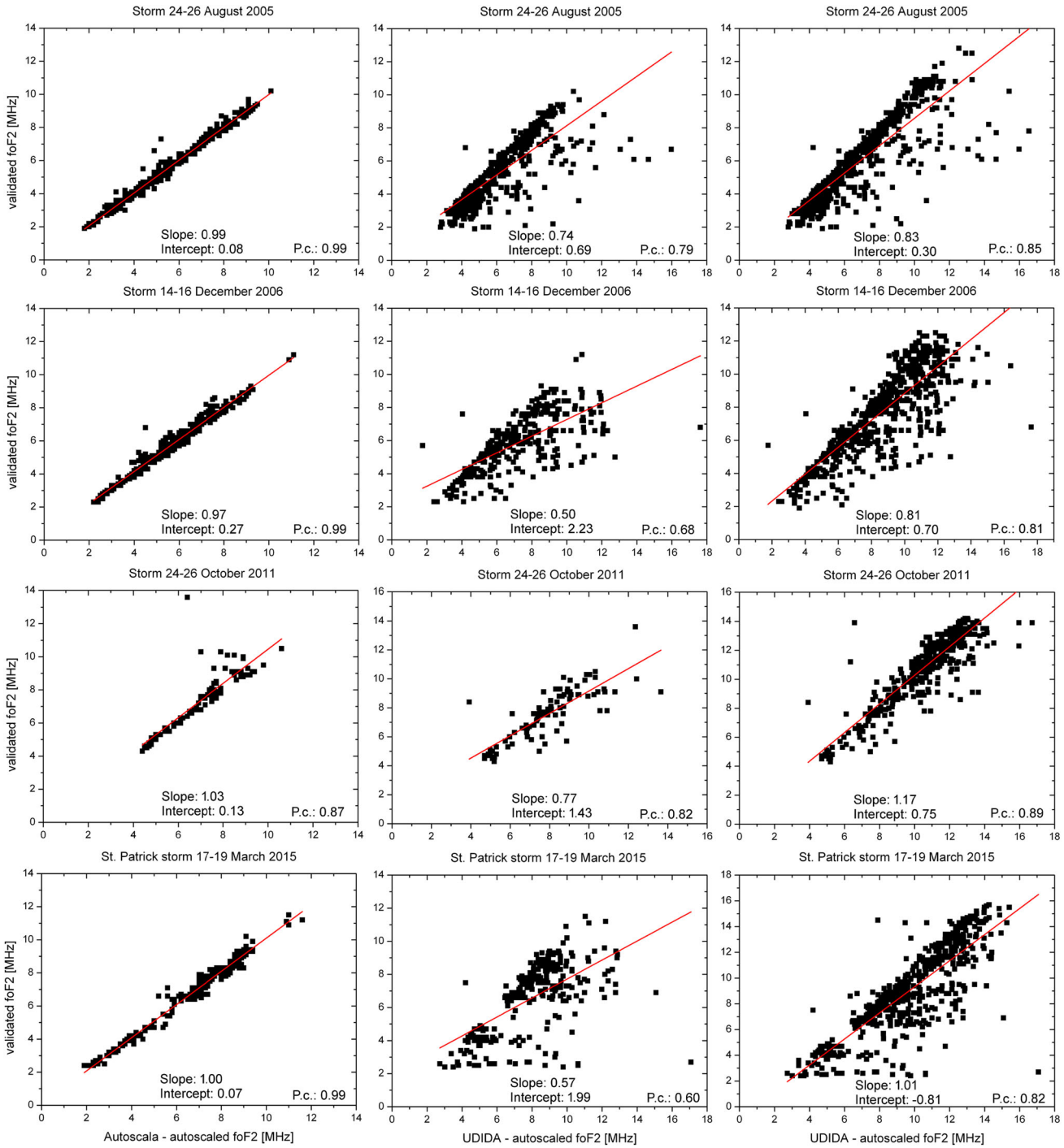

Fig. 3 Same as Fig. 2 but for the disturbed periods that occurred during 24–26 August 2005, 14–16 December 2006, 24–26 October 2011, and 17–19 March 2015

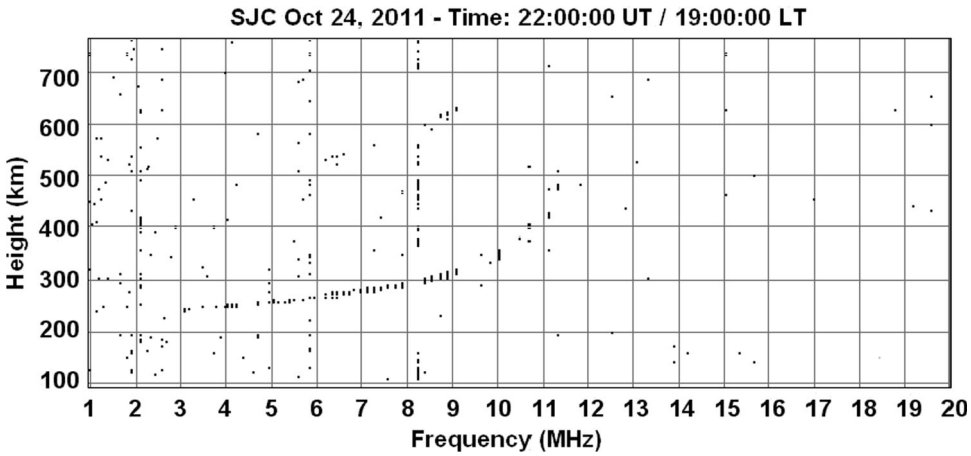

Fig. 4 Example of ionogram for which the operator scales a value of 11.0 MHz for *fo*F2, while Autoscala does not give any value as output

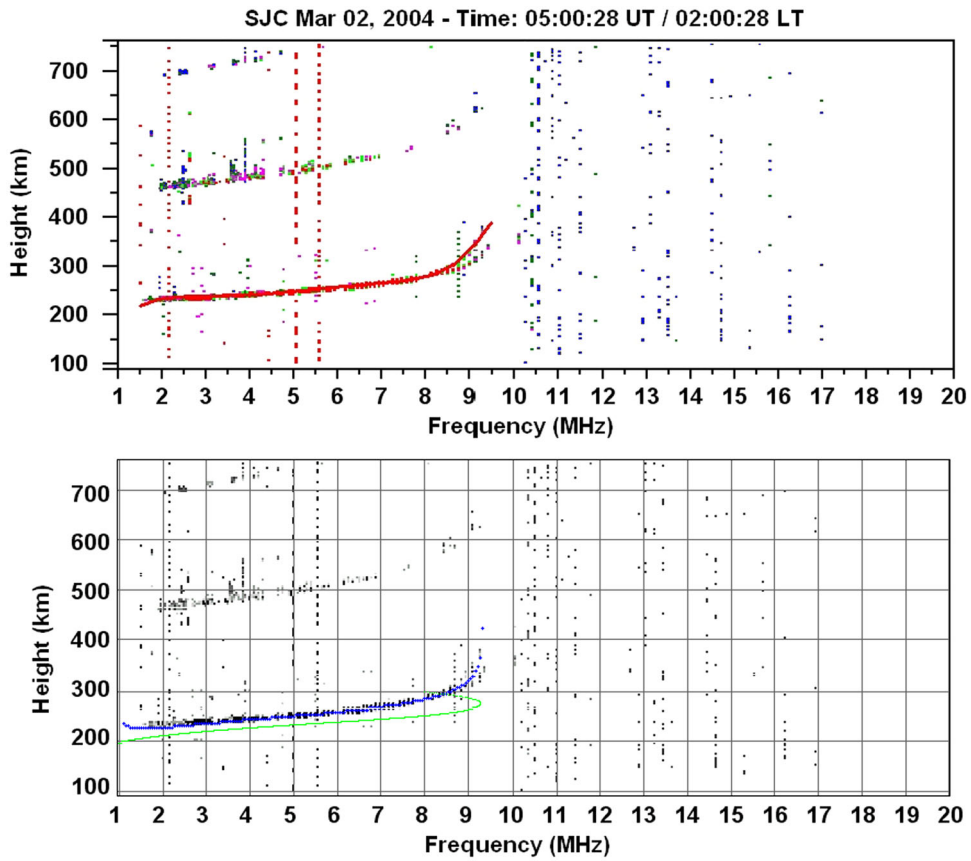

Fig. 5 Example of ionogram of subset 1 as autoscaled by (*top*) UDIDA and (*bottom*) Autoscala. The *red* curve in the *top panel* is the ionogram reconstructed by UDIDA, while the *blue* and the *green* curves in the *bottom panel* are, respectively, the ionogram reconstructed and the corresponding vertical electron density profile given by Autoscala

autoscaling is very high for Autoscala, independent of both the considered period and solar activity, while UDIDA shows an accuracy decrease both for disturbed periods, mainly because of the presence of multiple reflections of the sporadic E layer, multiple reflections of the F layer, and spread-F, and for nighttime ionograms because of noise. The main shortcomings showed by Autoscala are instead related to the inability in identifying the ionogram when this is characterized by a pronounced weakness of the trace, the presence of spread-F, and the appearance of additional stratifications of the F layer.

To smooth the aforementioned autoscaling errors made by both systems, so that they can produce more

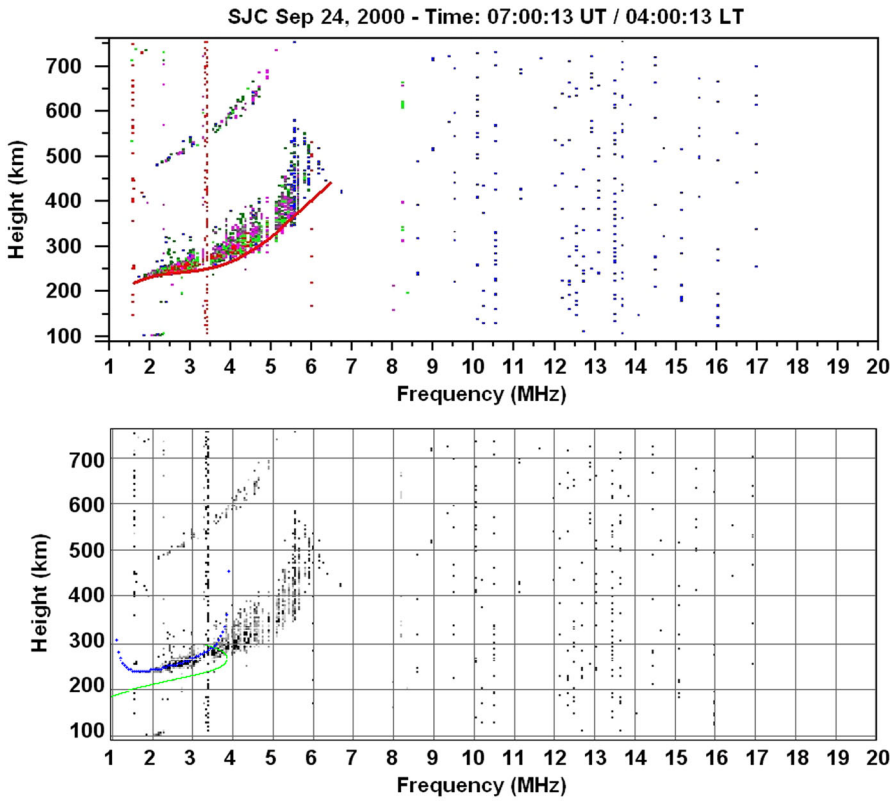

Fig. 6 Same as Fig. 5 but for an ionogram of subset 3

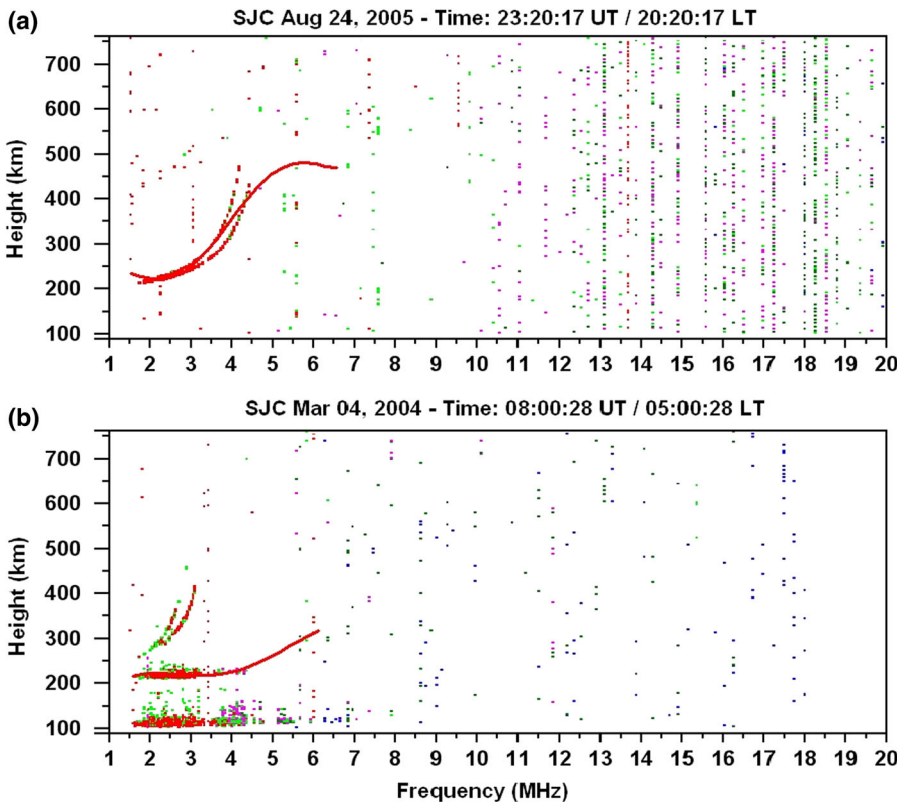

Fig. 7 Example of nighttime ionograms for which UDIDA was misled by: **a** the presence of noise characterizing the ionogram trace, and **b** the appearance of multiple reflections of the Es layer

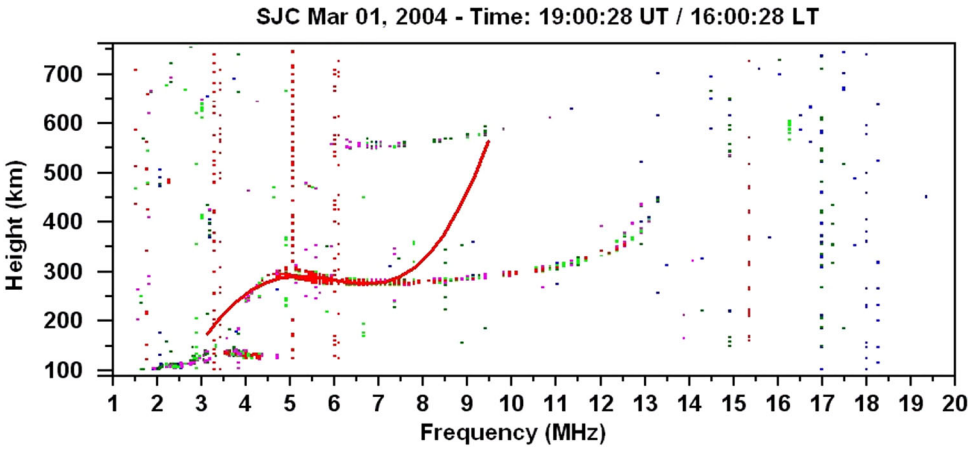

Fig. 8 Example of ionogram for which UDIDA was misled by the appearance on the ionograms of multiple reflections of the F layer

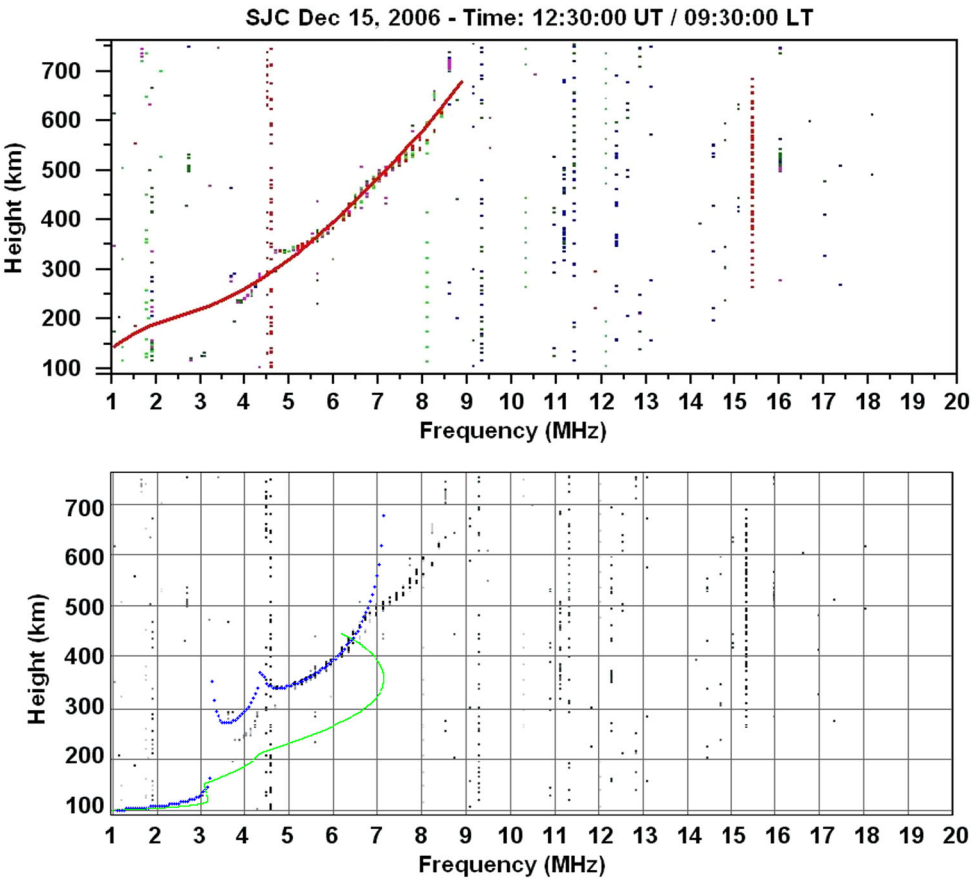

Fig. 9 Example of ionogram characterized by the appearance of additional stratifications of the F layer for which (*top*) UDIDA gives as output a reliable value of *fo*F2, while (*bottom*) Autoscala performs a strong underestimation of it

reliable *fo*F2 values, further fine-tuning analysis is needed. This can lead to the development of a reliable real-time monitoring system of the *fo*F2 ionospheric characteristic at SJC.

References

Astafyeva E, Zakharenkova I, Förster M (2015) Ionospheric response to the 2015 St. Patrick's Day storm: a global multi-instrumental overview. J Geophys Res 120(10):9023–9037. doi:10.1002/2015JA02629

Bamford RA, Stamper R, Cander LR (2008) A comparison between the hourly autoscaled and manually scaled characteristics from the Chilton ionosonde from 1996 to 2004. Radio Sci 43(1):RS1001. doi:10.1029/2005RS003401

Bullett T, Malagnini A, Pezzopane M, Scotto C (2010) Application of Autoscala to ionograms recorded by the VIPIR ionosonde. Adv Space Res 45(9):1156–1172. doi:10.1016/j.asr.2010.01.024

Carter BA, Yizengaw E, Pradipta R, Retterer JM, Groves K, Valladares C, Caton R, Bridgwood C, Norman R, Zhang K (2016) Global equatorial plasma bubble occurrence during the

2015 St. Patrick's Day storm. J Geophys Res 121(1):894–905. doi:10.1002/2015JA022194

Chartier AT, Matsuo T, Anderson JL, Collins N, Hoar TJ, Lu G, Mitchell CN, Coster AJ, Paxton LJ, Bust GS (2016) Ionospheric data assimilation and forecasting during storms. J Geophys Res 121(1):764–778. doi:10.1002/2014JA020799

Chen Z, Wang S, Zhang S, Fang G, Wang J (2013) Automatic scaling of F layer from ionograms. Radio Sci 48(3):334–343. doi:10.1002/rds.20038

Conkright RO, McNamara LF (1997) Quality control of automatically scaled vertical incidence ionogram data. Radio Sci 32(5):1997–2002. doi:10.1029/97RS01031

De Michelis P, Consolini G, Tozzi R, Marcucci MF (2016) Observations of high-latitude geomagnetic field fluctuations during St. Patrick's Day storm: Swarm and SuperDARN measurements. Earth Planets Space 68(105):1–16. doi:10.1186/s40623-016-0476-3

Ding Z, Ning B, Wan W, Liu L (2007) Automatic scaling of F2-layer parameters from ionograms based on the empirical orthogonal function (EOF) analysis of ionospheric electron density. Earth Planets Space 59(1):51–58. doi:10.1186/BF03352022

Enell C-F, Kozlovsky A, Turunen T, Ulich T, Välitalo S, Scotto C, Pezzopane M (2016) Comparison between manual scaling and Autoscala automatic scaling applied to Sodankylä Geophysical Observatory ionograms. Geosci Instrum Method Data Syst 5:53–64. doi:10.5194/gi-5-53-2016

Fagundes PR, Klausner V, Sahai Y, Pillat VG, Becker-Guedes F, Bertoni FCP, Bolzan MJA, Abalde JR (2007) Observations of daytime F2-layer stratification under the southern crest of the equatorial ionization anomaly region. J Geophys Res 112(A4):A04302. doi:10.1029/2006JA011888

Fox MW, Blundell C (1989) Automatic scaling of digital ionograms. Radio Sci 24(6):747–761. doi:10.1029/RS024i006p00747

Galkin IA, Reinisch BW (2008) The new ARTIST 5 for all digisondes, Ionosonde Netw Adv Group Bull 69. http://www.ips.gov.au/IPSHosted/INAG/web-69/2008/artist5-inag.pdf

Galkin IA, Reinisch BW, Huang X, Bilitza D (2012) Assimilation of GIRO data into a real-time IRI. Radio Sci 47(4):RS0L07. doi:10.1029/2011RS004952

Gardner LC, Schunk RW, Scherliess L, Sojka JJ, Zhu L (2014) Global assimilation of ionospheric measurements-Gauss Markov model: improved specifications with multiple data types. Space Weather 12(12):675–688. doi:10.1002/2014SW001104

Gilbert JD, Smith RW (1988) A comparison between the automatic ionogram scaling system ARTIST and the standard manual method. Radio Sci 23(6):968–974. doi:10.1029/RS023i006p00968

Igi S, Nozaki K, Nagayama M, Ohtani A, Kato H, Igarashi K (1993) Automatic ionogram processing systems in Japan. In: Proceedings of Session G6, 24th General Assembly of the International Union of Radio Science (URSI), 25 August–2 September 1993, Kyoto

Jacobs L, Poole AWV, McKinnel LA (2004) An analysis of automatically scaled F1 layer data over Grahamstown, South Africa. Adv Space Res 34(9):1949–1952. doi:10.1016/j.asr.2004.06.009

Jiang C, Yang G, Zhao Z, Zhang Y, Zhu P, Sun H (2013) An automatic scaling technique for obtaining F2 parameters and F1 critical frequency from vertical incidence ionograms. Radio Sci 48(6):739–751. doi:10.1002/2013RS005223

Jiang C, Yang G, Zhao Z, Zhang Y, Zhu P, Sun H, Zhou C (2014) A method for the automatic calculation of electron density profiles from vertical incidence ionograms. J Atmos Sol Terr Phys 107:20–29. doi:10.1016/j.jastp.2013.10.012

Jiang C, Zhang Y, Yang G, Zhu P, Sun H, Cui X, Song H, Zhao Z (2015a) Automatic scaling of the sporadic E layer and removal of its multiple reflection and backscatter echoes for vertical incidence ionograms. J Atmos Sol Terr Phys 129:41–48. doi:10.1016/j.jastp.2015.04.005

Jiang C, Yang G, Lan T, Zhu P, Song H, Zhou C, Cui X, Zhao Z, Zhang Y (2015b) Improvement of automatic scaling of vertical incidence ionograms by simulated annealing. J Atmos Sol Terr Phys 133:178–184. doi:10.1016/j.jastp.2015.09.002

Krasheninnikov I, Pezzopane M, Scotto C (2010) Application of Autoscala to ionograms recorded by the AIS-Parus ionosonde. Comp Geosci 36(5):628–635. doi:10.1016/j.cageo.2009.09.013

Lee IT, Matsuo T, Richmond AD, Liu JY, Wang W, Lin CH, Anderson JL, Chen MQ (2012) Assimilation of FORMOSAT-3/COSMIC electron density profiles into a coupled thermosphere/ionosphere model using ensemble Kalman filtering. J Geophys Res 117(A10):A10318. doi:10.1029/2012JA017700

Lynn KJW, Harris TJ, Sjarifudin M (2000) Strattification of the F2 layer observed in Southeast Asia. J Geophys Res 105(A12):27147–27156. doi:10.1029/2000JA900056

MacDougall JW, Grant IF, Shen X (1993) The Canadian advanced digital ionosonde: design and results. In: Proceedings of 24th General Assembly of the International Union of Radio Science (URSI), 25 August–2 September 1993, Kyoto

McNamara LF (2006) Quality figures and error bars for autoscaled Digisonde vertical incidence ionograms. Radio Sci 41(4):RS4011. doi:10.1029/2005RS003440

McNamara LF, Angling MJ, Elvidge S, Fridman SV, Hausman MA, Nickisch LJ, McKinnell LA (2013) Assimilation procedures for updating ionospheric profiles below the F2 peak. Radio Sci 48(2):143–157. doi:10.1002/rds.20020

Nava B, Rodríguez-Zuluaga J, Alazo-Cuartas K, Kashcheyev A, Migoya-Orué Y, Radicella SM, Amory-Mazaudier C, Fleury R (2016) Middle-and low-latitude ionosphere response to 2015 St. Patrick's Day geomagnetic storm. J Geophys Res 121(4):3421–3438. doi:10.1002/2015JA022299

Nayak C, Tsai L-C, Su S-Y, Galkin IA, Tan ATK, Nofri E, Jamjareegulgarn P (2016) Peculiar features of the low-latitude and midlatitude ionospheric response to the St. Patrick's Day geomagnetic storm of 17 March 2015. J Geophys Res 121(8):7941–7960. doi:10.1002/2016JA022489

Pezzopane M (2004) Interpre: a Windows software for semiautomatic scaling of ionospheric parameters from ionograms. Comp Geosci 30(1):125–130. doi:10.1016/j.cageo.2003.09.009

Pezzopane M, Scotto C (2004) Software for the automatic scaling of critical frequency foF2 and MUF(3000)F2 from ionograms applied at the Ionospheric Observatory of Gibilmanna. Ann Geophys 47(6):1783–1790

Pezzopane M, Scotto C (2005) The INGV software for the automatic scaling of foF2 and MUF(3000)F2 from ionograms: a performance comparison with ARTIST 4.01 from Rome data. J Atmos Sol Terr Phys 67(12):1063–1073. doi:10.1016/j.jastp.2005.02.022

Pezzopane M, Scotto C (2007) Automatic scaling of critical frequency foF2 and MUF(3000)F2: a comparison between Autoscala and ARTIST 4.5 on Rome data. Radio Sci 42(4):RS4003. doi:10.1029/2006RS003581

Pezzopane M, Scotto C (2010) Highlighting the F2 trace on an ionogram to improve Autoscala performance. Comp Geosci 36(9):1168–1177. doi:10.1016/j.cageo.2010.01.010

Pezzopane M, Scotto C, Tomasik Ł, Krasheninnikov I (2010) Autoscala: an aid for different ionosondes. Acta Geophys 58(3):513–526. doi:10.2478/s11600-009-0038-1

Pezzopane M, Pietrella M, Pignatelli A, Zolesi B, Cander LR (2011) Assimilation of autoscaled data and regional and local ionospheric models as input sources for real-time 3-D International Reference Ionosphere modeling. Radio Sci 46(5):RS5009. doi:10.1029/2011RS004697

Pezzopane M, Pietrella M, Pignatelli A, Zolesi B, Cander LR (2013) Testing the three-dimensional IRI-SIRMUP-P mapping of the ionosphere for disturbed periods. Adv Space Res 52(10):1726–1736. doi:10.1016/j.asr.2012.11.028

Piggott WR, Rawer K (1972) U.R.S.I. Handbook of Ionogram Interpretation and Reduction. World Data Center A for Solar-Terrestrial Physics, NOAA, Boulder

Pignalberi A, Pezzopane M, Tozzi R, De Michelis P, Coco I (2016) Comparison between IRI and preliminary Swarm Langmuir probe measurements during the St. Patrick storm period. Earth Planets Space 68(93):1–18. doi:10.1186/s40623-016-0466-5

Pillat VG, Guimaraes LNF, Fagundes PR, da Silva JDS (2013) A computational tool for ionosonde CADI's ionogram analysis. Comp Geosci 52:372–378. doi:10.1016/j.cageo.2012.11.009

Pillat VG, Fagundes PR, Guimaraes LNF (2015) Automatically identification of Equatorial Spread-F occurrence on ionograms. J Atmos Sol Terr Phys 135:118–125. doi:10.1016/j.jastp.2015.10.015

Reinisch BW, Huang X (1983) Automatic calculation of electron density profiles from digital ionograms: 3. Processing of bottomside ionograms. Radio Sci 18(3):477–492. doi:10.1029/RS018i003p00477

Reinisch BW, Huang X, Galkin IA, Paznukhov V, Kozlov A (2005) Recent advances in real-time analysis of ionograms and ionospheric drift measurements with digisondes. J Atmos Sol Terr Phys 67(12):1054–1062. doi:10.1016/j.jastp.2005.01.009

Sabbagh D, Scotto C, Sgrigna V (2016) A regional adaptive and assimilative three-dimensional ionospheric model. Adv Space Res 57(5):1241–1257. doi:10.1016/j.asr.2015.12.038

Scotto C (2009) Electron density profile calculation technique for Autoscala ionogram analysis. Adv Space Res 44(6):756–766. doi:10.1016/j.asr.2009.04.037

Scotto C, MacDougall J (2012) Application of Autoscala software to the Canadian advanced digital ionosonde. Int J Remote Sens 33(17):5574–5582. doi:10.1080/01431161.2012.661097

Scotto C, Pezzopane M (2008) Removing multiple reflections from the F2 layer to improve Autoscala performance. J Atmos Sol Terr Phys 70(15):1929–1934. doi:10.1016/j.jastp.2008.05.012

Spogli L, Cesaroni C, Di Mauro D, Pezzopane M, Alfonsi L, Musicò E, Povero G, Pini M, Dovis F, Romero R, Linty N, Abadi P, Nuraeni F, Husin A, Le Huy M, Thi Lan T, Vihn La T, Pillat VG, Floury N (2016) Formation of ionospheric irregularities over Southeast Asia during the 2015 St. Patrick's Day storm. J Geophys Res 121(12):12211–12233. doi:10.1002/2016JA023222

Stankov SM, Jodogne JC, Kutiev I, Stegen K, Warnant R (2012) Evaluation of automatic ionogram scaling for use in real-time ionospheric density profile specification: dourbes DGS-256/ARTIST-4 performance. Ann Geophys 55(2):283–291. doi:10.4401/ag-4976

Su F, Zhao Z, Li S, Yao M, Chen G, Zhou Y (2012) Signal identification and trace extraction for the vertical ionogram. IEEE Geosci Remote Sens Lett 9(6):1031–1035. doi:10.1109/LGRS.2012.2189350

Tsai LC, Berkey FT (2000) Ionogram analysis using fuzzy segmentation and connectedness techniques. Radio Sci 35(5):1173–1186. doi:10.1029/1999RS002170

Tulasi Ram S, Yokoyama T, Otsuka Y, Shiokawa K, Sripathi S, Veenadhari B, Heelis R, Ajith KK, Gowtam VS, Gurubaran S, Supnithi P, Le Huy M (2016) Duskside enhancement of equatorial zonal electric field response to convection electric fields during the St. Patrick's Day storm on 17 March 2015. J Geophys Res 121(1):538–548. doi:10.1002/2015JA021932

Zabotin NA, Wright JW, Zhbankov GA (2006) NeXtYZ: three-dimensional electron density inversion for dynasonde ionograms. Radio Sci 41(6):RS6S32. doi:10.1029/2005RS003352

Zheng H, Ji G, Wang G, Zhao Z, He S (2013) Automatic scaling of F layer from ionograms based on image processing and analysis. J Atmos Sol Terr Phys 105–106:110–118. doi:10.1016/j.jastp.2013.09.007

Zhong J, Wang W, Yue X, Burns AG, Dou X, Lei J (2016) Long-duration depletion in the topside ionospheric total electron content during the recovery phase of the March 2015 strong storm. J Geophys Res 121(5):4733–4747. doi:10.1002/2016JA022469